URSI AP-RASC 2019, New Delhi, India; 09 - 15 March 2019

Probe Positioning Error Sensitivity Analysis for Planar Near-field Antenna Measurements

S. G. H. Kriel*(1), D. I. L. de Villiers(1)
(1) Dept. of E&E Engineering, Stellenbosch University, Matieland, 7600, South Africa

Abstract

Unmanned aerial vehicle based field measurements have been proposed as a possible solution to provide calibration data for large ground based radio telescope arrays, such as the Mid Frequency Aperture Array planned for the Square Kilometre Array project. This paper considers planar near-field scanning using a quad-copter equipped with a differential GPS (DGPS). The effect of random positional errors associated with DGPS on two different near- to far-field (FF) transformations, namely the planar plane wave expansion (PPWE) and the Fast Irregular Antenna Field Transformation Algorithm (FIAFTA), are investigated in the frequency range 450 MHz–1450 MHz. It is shown that FIAFTA drastically outperforms the PPWE for the given situation and produces adequate results over the band for a positional error of 1 cm. However, considering positional inaccuracies of 5 cm, both algorithms produce a predicted FF pattern which is corrupted beyond being of any practical use.

1 Introduction

Proposed designs for the Mid Frequency Aperture Array (MFAA), such as that in [1], present new challenges with regard to pattern calibration, chief among these being the unprecedented number of elements projected to feature in the instrument. With a wide field of view (FoV), coupled with a possible lack of natural calibration sources in the observation domain, traditional calibration methods become problematic. Given this, interest into unmanned aerial vehicles (UAVs), acting as artificial calibration sources, has arisen as a possible solution. Direct far-field (FF) measurements of various antenna systems using UAVs, such as that in [2], have been reported to achieve reasonable accuracy. However, the proposed aperture size of the MFAA gives a FF region at distances which place unreasonable requirements on the battery life of the UAV. Therefore, this study focuses on near-field (NF) measurements of an artificial source in the form of a quad-copter with two orthogonal transmitting dipole antennas and on-board differential GPS (DGPS). To be of use in calibrating a radio telescope, the measured NF must be transformed into the FF pattern of the antenna under test (AUT) using a suitable transformation algorithm. This requires knowledge of both magnitude and phase of the NF. This additional phase requirement makes NF measurements more sensitive to probe positioning errors than FF measurements. As such, two NF to FF transforms are applied in this study and their sensitivity to positional errors associated with a typical DGPS (taken to be between 1 cm–5 cm) is compared in the frequency band of interest 450 MHz–1450 MHz. The first transformation is the well-known planar plane wave expansion (PPWE), which makes use of the fast Fourier transform (FFT). A positional error sensitivity analysis, akin to that undertaken here, utilising the PPWE was performed in [3] and showed that accurate FF pattern characterisation, over this frequency band and for the given measurement system, is implausible. Therefore, we now extend this analysis by comparing the performance of the PPWE against the Fast Irregular Antenna Field Transformation Algorithm (FIAFTA), recently developed by Eibert et al. and described in [4], [5] and [6]. As the name suggests, FIAFTA does not necessitate the regularly spaced sample grid required by FFT based algorithms such as the PPWE. This makes FIAFTA an attractive choice for UAV based measurements, where measurement data positions are, by nature, arbitrary. In addition, it is the hope that FIAFTA's relaxation on sample spacing requirements will make for an FF pattern prediction that is more resilient to probe positional errors than the PPWE. Such a comparison between the two algorithms' sensitivity to probe positional errors is carried out in [5], where it appears that both algorithms are equally sensitive. However, the positional error levels used were far smaller than those of interest here.

2 Nearfield to Farfield Transforms

2.1 Planar Plane Wave Expansion

A well-known and mathematically simple method for calculating the FF from a planar NF measurement is to utilise the FFT to compute a spectrum of plane waves, propagating from an aperture plane above the AUT. This is done by measuring the tangential **E**-field components (E_{xa} and E_{ya}) over a plane, a fixed distance $z = z_0$ from the AUT. The FFT is then used to calculated the $\hat{x}$ and $\hat{y}$ components of the plane wave spectra as [7]

$$f_x(k_x,k_y) = \mathscr{F}\{E_{xa}\}, \quad f_y(k_x,k_y) = \mathscr{F}\{E_{ya}\}, \qquad (1)$$

where $\mathscr{F}$ denotes the Fourier transform and the wave vector is defined in Cartesian coordinates as $\mathbf{k} = k_x\hat{x} + k_y\hat{y} + k_z\hat{z}$. Utilising the method of stationary phase, the spherical components of the **E**-field in the FF region can then be approx-

imated as

$$E_\theta^{FF}(r,\theta,\phi) \approx j\frac{ke^{-jkr}}{r}(f_x\cos(\phi)+f_y\sin(\phi)), \quad (2)$$

$$E_\phi^{FF}(r,\theta,\phi) \approx j\frac{ke^{-jkr}}{r}\cos(\theta)(-f_x\sin(\phi)+f_y\cos(\phi)), \quad (3)$$

at a radial distance r away from the AUT. Here we will investigate the accuracy of the predicted total **E**-field magnitude in the FF, calculated as

$$E_{total}^{FF}(r,\theta,\phi) = \sqrt{|E_\theta^{FF}|^2+|E_\phi^{FF}|^2}. \quad (4)$$

Using the FFT imposes strict requirements on the planarity and regularity of the sample space and any deviation in this causes significant errors in the predicted FF pattern. Additionally, in order to fully recover the pattern, a Nyquist sampling criterion of $\Delta x = \Delta y = \lambda/2$, with λ being the wavelength, should be adhered to.

2.2 FIAFTA

The strict sample spacing requirements of FFT based algorithms pose significant obstacles for UAV measurements, where perfect samples on a regular grid are not a reality. Therefore, transformation algorithms more suitable to arbitrary NF samples are desirable. FIAFTA is such an algorithm, where the diagonal translation operator, T_L, well-known from the fast multipole method (FMM) [8] as

$$T_L(\hat{k},\hat{r}_M) = -\frac{jk}{4\pi}\sum_{l=0}^{L}(-j)^l(2l+1)\mathrm{h}_l^{(2)}(kr_M)\mathrm{P}_l(\hat{k}\cdot\hat{r}_M), \quad (5)$$

is used to relate propagating plane waves emanating from the AUT into incoming plane waves at the probe, for each measurement point $\mathbf{r}_M$. Here $\mathrm{h}_l^{(2)}$ denotes the second order spherical Hankel function, P_l is a Legendre polynomial and L is the number of multipole terms, which must be chosen according to the size of the AUT and probe. Here we assume an ideal probe and choose L according to [5]

$$L = \frac{kd}{2}+10, \quad (6)$$

with d being the diameter of the minimum sphere enclosing the AUT. Utilising (5), it is possible to represent the voltage measured on two orthogonal measurement probes (U^1 and U^2) as the k-space integral of plane wave currents, $\tilde{\mathbf{J}}$, over the Ewald sphere of the AUT [4]. Using numerical quadrature to perform the integral, the probe voltage at each measurement point can be expressed as

$$U^{1/2}(\phi_m,\theta_n,r_M) = -j\frac{\omega\mu}{4\pi}\sum_{k_\phi}\sum_{k_\theta}T_L(\hat{k},\hat{r}_M)W(k_\theta) \times \mathbf{P}^{1/2}(k_\phi,k_\theta,\phi_m,\theta_n)\cdot(\bar{\mathbf{I}}-\hat{k}\hat{k})\cdot\tilde{\mathbf{J}}(k_\phi,k_\theta). \quad (7)$$

Here, each sample location is represented by $m=[1,...,M]$ and $n=[1,...,N]$, where M and N are the number of NF samples in the $\hat{\phi}$ and $\hat{\theta}$ directions respectively. $\bar{\mathbf{I}}$ is the unit dyad and **P** is the FF pattern of the probe (assumed ideally isotropic in this paper). The weighting function $W(k_\theta)$, as well as the discrete representation of plane wave-numbers as k_{ϕ_p} and k_{θ_q}, where $p=[1,...,P]$ and $q=[1,...,Q]$, is determined by a suitable quadrature rule. The number of plane wave samples in the $\hat{\phi}$ and $\hat{\theta}$ directions (P and Q) set up by the quadrature rule are in turn a function of the multipole order of the AUT, calculated as in (6). With (7), it is possible to set up the linear system of equations

$$\mathbf{U}' = -j\frac{\omega\mu}{4\pi}||C||\cdot\tilde{\mathbf{J}}', \quad (8)$$

where the coupling matrix C contains the translation operator, quadrature weighting function and probe receiving FF pattern,

$$C_{\theta/\phi}^{1/2}(k_{\phi p},k_{\theta q},\phi_m,\theta_n) = T_L(\hat{k},\hat{r}_M)W(k_{\theta_q}) \times P_{\phi/\theta}^{1/2}(k_{\phi_p},k_{\theta_q},\phi_m,\theta_n). \quad (9)$$

A suitable solver, such as the generalised minimal residual (GMRES) solver, is then used to solve the corresponding normal system of (8) for the plane wave currents tangential to the Ewald sphere. The FF may then be approximated as

$$\mathbf{E}^{FF}(r,\theta,\phi) = -j\frac{\omega\mu}{4\pi}\frac{e^{-jkr}}{r}\tilde{\mathbf{J}}(k_\theta,k_\phi), \quad (10)$$

The preconfigured tolerance of the GMRES solver (which dictates the desired residuum of the final solution) is an important factor, especially when considering measurement data corrupted by noise. In this case it is preferable to set a higher tolerance level in order to terminate the solver before the solution is severely affected by noise [4]. In addition to this, the poles of the Ewald sphere, i.e. at $\theta=0$ and $\theta=\pi$, require special attention if good convergence results are to be achieved. This is due to the fact that these points present discontinuities in spherical coordinates and must be appropriately handled during the numerical integration. In [6] the Cartesian vector components are considered as they present continuous functions over the surface and here we follow a similar approach, whereby the measured $\hat{x}$ and $\hat{y}$ components of the NF are used to resolve the plane wave currents, $\tilde{J}_x$ and $\tilde{J}_y$, over the Ewald sphere. From this the $\hat{z}$-directed plane wave currents, $\tilde{J}_z$, are solved using the relation [7]

$$\tilde{J}_z(k_x,k_y) = -\frac{k_x\tilde{J}_x(k_x,k_y)+k_y\tilde{J}_y(k_x,k_y)}{k_z}, \quad (11)$$

from which the spherical components and/or total magnitude of the FF, as per (4), can be readily determined.

3 Experimental Procedure

3.1 Antenna Under Test

An $\hat{x}$-directed half-wave dipole, situated $\lambda/4$ above an infinite ground plane, is considered as it mimics the wide FoV of the MFAA. The method of images is used to remove the

plane and the equivalent system is simulated in FEKO [9]. As the effects of non-ideal probes are not considered here, the $\hat{x}$ and $\hat{y}$ components of the NF on a planar surface is calculated directly and used in the appropriate transformation. For the PPWE, a square sampling plane with side lengths of 10 m, a distance $z_0 = 3\lambda$ from the dipole was calculated at a Nyquist sampling rate. For FIAFTA, a spherical sample spacing projected onto the plane at z_0, as detailed in [5], is used for the same amount of samples as in the PPWE. With a multipole order chosen as $L = 14$, the amount of measurement points greatly exceeds the number of unknowns, helping to create a heavily overdetermined system, which may be more resilient to noise. Additionally, in an attempt to limit the affect of noise on the solution, the tolerance of the GMRES solver is set to the relatively high value of 10^{-3}.

3.2 Error Calculation

To investigate the sensitivity of the transformations to positional error, noise is injected into the NF measurement coordinates (x,y,z) to give the noisy coordinates

$$(x_n, y_n, z_n) = (x+n_x, y+n_y, z+n_z), \tag{12}$$

where n_x, n_y and n_z are randomly chosen from a normal distribution with mean centred on the measurement location and standard deviation (σ) determining the level of error. Taking NF measurements at these noisy coordinates, the transformed FF is calculated for both algorithms as if measurement coordinates were ideal, thus simulating erroneous measurements taken by a UAV. The total magnitude of the transformed FF at a radial distance $r = 100$ m is then compared to a reference, E_{REF}, which is the direct FF measurement taken from FEKO. This gives an error map, normalised to the reference, as

$$e_k(\theta,\phi) = \frac{|E_{REF}(\theta,\phi) - E^{FF}_{total}(\theta,\phi)|}{E_{REF}(\theta,\phi)}, \tag{13}$$

over the entire region. We go on to analyse the root mean square (RMS) error over multiple runs, N, given as

$$e_{RMS}(\theta,\phi) = \sqrt{\frac{1}{N}\sum_{k=1}^{N}(e_k(\theta,\phi))^2}, \tag{14}$$

and the maximum error

$$e_{max}(\theta,\phi) = max(\mathbf{e}(\theta,\phi)), \tag{15}$$

where $\mathbf{e}(\theta,\phi)$ is the vector $[e_1, e_2, ..., e_N]$ and $max()$ takes the maximum error seen, over N runs, at each FF angle. These error maps are reduced to scalars by integrating over the FoV of interest (here taken as within 60° from zenith) and normalised to the FoV surface area (S),

$$S = \pi(\sin^2(\frac{\pi}{3}) + (1 - \cos^2(\frac{\pi}{3})), \tag{16}$$

giving the scalar error e_i as [3]

$$e_i = \frac{1}{S}\int_0^{\pi}\int_{-\frac{\pi}{3}}^{\frac{\pi}{3}} e(\theta,\phi)\cos(\theta)d\theta d\phi. \tag{17}$$

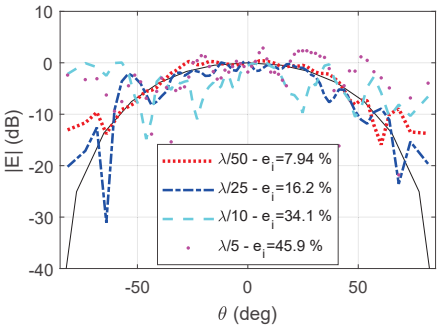

(a) PPWE

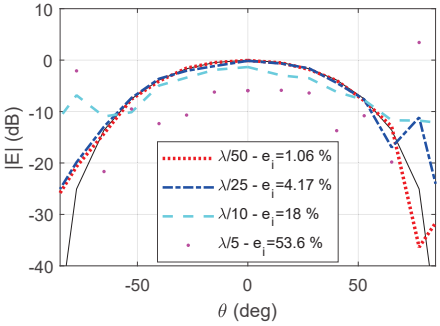

(b) FIAFTA

Figure 1. Transformed FF at $\phi = 0°$ for varying positional error, where the black line represents the reference FF

Equation (17) provides a metric which can be used to easily compare the performance of the two algorithms when subjected to varying levels of positional error.

4 Results

The effect of varying levels of positional error, $\lambda/50 < \sigma < \lambda/5$, in the transformed FF for both the PPWE and FIAFTA can be seen in Fig. 1a and Fig. 1b respectively. The calculated FF error (e_i) for each injected positional error is shown in the legend so that one can reconcile this metric with the affected pattern plot. One can immediately see that FIAFTA appears to be more stable when the positional error is within a tenth of a wavelength. Above this and FIAFTA is seen to give higher error levels than the PPWE, a fact demonstrated in Fig. 2, which compares the maximum and RMS error of the two algorithms for increasing σ. It is seen that FIAFTA performs better only up to around $\sigma = 0.22\lambda$, after which the PPWE presents a lower RMS error. This behaviour is of little significance considering the fact that, at these high error levels, both transformed FF patterns are corrupted beyond being able to serve any practical purpose. To investigate the plausibility of NF measurements taken with the UAV system in question, upper and lower positional error levels are defined as $\sigma_{lower} = 1$ cm and $\sigma_{upper} = 5$ cm, which correspond to typical levels seen in DGPS. From this, the upper and lower bounds of the maximum FF error (e_{max} converted to a scalar via (17)) is

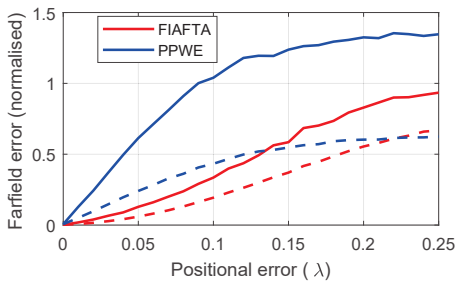

Figure 2. Comparing maximum (solid) and RMS (dotted) error for increasing positional error

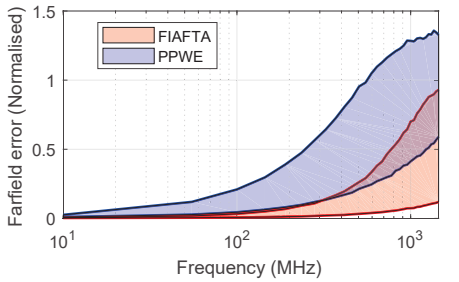

Figure 3. Comparison of maximum FF error bounds (e_{max}) for a positional error between 1 cm–5 cm

computed for 50 runs ($N = 50$) over the frequency range 10 MHz–1450 MHz. The performance of the two algorithms is compared in Fig. 3, where FIAFTA is seen to give lower error levels over the whole band.

5 Conclusion

It is clear from the above analysis that, for the given situation, FIAFTA presents a superior alternative to the PPWE. For $\sigma = 5$ cm, we find that using current DGPS technology with the PPWE is completely implausible above 100 MHz and largely unsatisfactory below 100 MHz. Contrary to this, FIAFTA produces adequate results below 100 MHz, with a maximum error of around 3% at 100 MHz. As we approach our band of interest, the maximum error is seen to rise to 23% at 450 MHz and beyond this FIAFTA produces unusable results. If, however, we could achieve a $\sigma = 1$ cm maximum positional error, NF measurements with DGPS over the whole band become possible with FIAFTA, where the error at 1450 MHz reaches a maximum of 12% (contrary to the PPWE which reaches 60% error for the same scenario). This improved performance of FIAFTA is seen as a result of the larger number of *effective* samples used by this method, i.e. for the same number of samples the FIAFTA system is overdetermined whereas the PPWE is not.

Aside from possible advances in DGPS technology, results may be improved by extending FIAFTA to include a multilevel FMM (MLFMM) type grouping scheme of measurement and source coordinates, as detailed in [4]. In addition to providing a more flexible algorithm, the aggregation procedures of the MLFMM may invoke an implicit averaging effect in the NF measurements, thus reducing FIAFTA's sensitivity to positional errors. FIAFTA also lends itself naturally to the use of spherical harmonic expansions and is able to utilise any *a priori* information available on the AUT. This, together with the possibility of averaging results over multiple runs or increasing the amount of NF samples, makes future pattern characterisation of the MFAA via UAV's equipped with DGPS realisable.

6 Acknowledgements

This research was supported by the South African Radio Astronomy Observatory, which is a facility of the National Research Foundation, an agency of the Department of Science and Technology (NRF Grant Numbers: 75322 and 106033).

References

[1] E. Colin-Beltran, A. J. Faulkner *et al.*, "Log-periodic sparse aperture array antennas dedicated to the MFAA instrument of the SKA telescope," in *Int. Conf. Electromag. Adv. Applic.*, Palm Beach, FL, Aug 2014, pp. 746–749.

[2] G. Virone, A. M. Lingua *et al.*, "Antenna pattern verification system based on a micro unmanned aerial vehicle (UAV)," *IEEE Antennas Wireless Propag. Lett.*, vol. 13, pp. 169–172, 2014.

[3] H. Pienaar and D. B. Davidson, "Error sensitivity analysis for multi-copter planar positioning on low-gain nearfield measurements," in *Int. Conf. Electromag. Adv. Applic.*, Cairns, Australia, Sept 2016, pp. 568–571.

[4] T. F. Eibert, E. Kilic *et al.*, "Electromagnetic field transformations for measurements and simulations," *Progress in Electromag. Res.*, vol. 151, pp. 127–150, 2015.

[5] M. A. Qureshi, "Near-field error analysis and efficient sampling techniques for the fast irregular antenna field transformation algorithm," Ph.D. dissertation, Technische Universität München, 2013.

[6] T. F. Eibert, "A diagonalized multilevel fast multipole method with spherical harmonics expansion of the k-space integrals," *IEEE Trans. Antennas Propag.*, vol. 53, no. 2, pp. 814–817, 2005.

[7] S. Gregson, J. McCormick *et al.*, *Principles of planar near-field antenna measurements*. IET, 2007, vol. 53.

[8] R. Coifman, V. Rokhlin *et al.*, "The fast multipole method for the wave equation: A pedestrian prescription," *IEEE Antennas Propag. Mag.*, vol. 35, no. 3, pp. 7–12, 1993.

[9] Altair Engineering Inc., "Altair FEKO 2017.2," Stellenbosch, South Africa, 2017. [Online]. Available: https://altairhyperworks.com/product/FEKO